Electrochemically Driven C-N Bond Formation from CO_2 and Ammonia at the Triple-Phase Boundary

Junnan Li[1] and Nikolay Kornienko[1]*

[1]Department of Chemistry, Université de Montréal, 1375 Avenue Thérèse-Lavoie-Roux, Montréal, QC H2V 0B3, Canada.

*E-mail: nikolay.kornienko@umontreal.ca

Abstract:

Electrosynthetic techniques are gaining prominence across the fields of chemistry, engineering and energy science. However, most works within the direction of synthetic heterogeneous electrocatalysis focus on water electrolysis and CO_2 reduction. In this work, we moved to expand the scope of this technology by developing a synthetic scheme which couples CO_2 and NH_3 at a gas-liquid-solid triple-phase boundary to produce species with C-N bonds. Specifically, by bringing in CO_2 from the gas phase and NH_3 from the liquid phase together over solid copper catalysts, we have succeeded in forming formamide and acetamide products for the first time. In a subsequent complementary step, we have combined electrochemical analysis and a newly developed *operando* spectroelectrochemical method, capable of probing the aforementioned triple phase boundary, to extract an initial level of mechanistic analysis regarding the reaction pathways of these reactions and the current system's limitations. We believe that the development and understanding of this set of reaction pathways will play an exceptionally significant role in expanding the community's understanding of on-surface electrosynthetic reactions as well as push this set of inherently sustainable technologies towards widespread applicability.

Introduction:

With the increased focus on attaining global sustainability as a means to mitigate climate change and environmental degradation, the development of green technologies to enable the transition is increasingly important. Within this context, renewable electricity-powered electrosynthetic routes towards generating the fuels and chemicals that drive modern society stand to play a significant role if they manage to displace currently used fossil-fuel dependent methods[1-3]. While the recent decade of academic research has largely focused on water electrolysis[4] and CO_2 reduction[5] to generate H_2 and carbon-based fuels, respectively, there is no reason that the scope of heterogeneous electrosynthesis needs to be limited to these reactions as in principle, almost any commodity chemical can be synthesized from abundant building blocks (N_2, H_2O, CH_4, biomass…) if the proper catalytic system would be developed. The difficulty in realizing this ambitious aim as that at this point, only relatively simple electrosynthetic reactions over heterogeneous catalysts are well-understood and can be carried out at high rates and selectivity.

To this end, we moved to develop electrosynthetic routes to C-N bond formation using CO_2 and NH_3 as model building blocks. In general, despite the biological, societal and technological importance of many chemicals containing C-N bonds[6-9], the area of electrochemical C-N bond formation is very nascent. While biological[10-12] and chemical[6,13] routes are established, only few examples exist in carrying out C-N coupling on heterogeneous electrocatalysts. Thus, new reaction schemes and mechanistic insights in this context stand to provide a significant boost to the community[14-20]. In the context of heterogeneous catalysis, ammonia has previously been synthesized from co-electrolysis of N_2 or nitrate together with CO_2[15,17,18,20]. α-keto acids have been converted into amino acids with hydroxylamine as a N-source.[21] Further, CO was co-electrolyzed with a series of different amines to generate amide products[16]. Finally, a host biomass-derived furans were reductively aminated to produce to amine derivatives[19]. To expand the scope of possibilities of heterogeneously catalyzed C-N bond formation, we have developed an electrosynthetic scheme in which NH_3 from the liquid phase would react with CO_2 from the gas phase over a heterogeneous Cu catalyst at a gas-liquid-solid triple-phase boundary (Fig.1). As such, we generated formamide and acetamide from CO_2 and NH_3 for the first time, opening up a new avenue to the research community. Through quantitative reaction analysis and newly-developed infrared spectroelectrochemical investigations, we have built up a set of mechanistic insights in terms of elucidating reaction pathways and performance limitations, thus enabling the rational design of next-generation electrosynthetic systems.

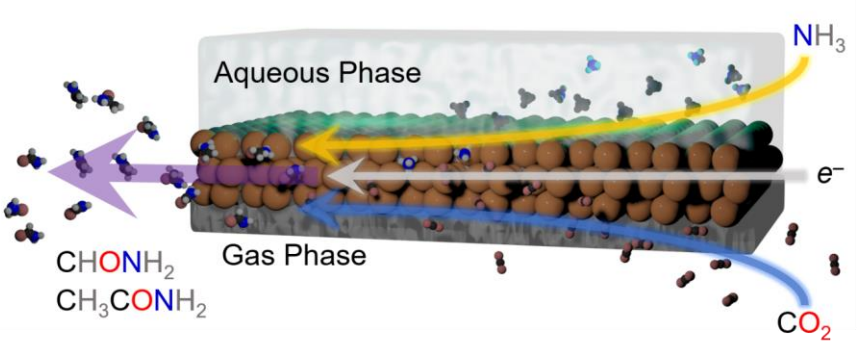

Figure 1: Illustration of electrosynthetic strategy for on-surface C-N bond formation.

Catalyst Construction:

As a starting point, we selected two types of commercially available copper catalysts, Cu and CuO nanoparticles, to use in our study. Copper was selected as the element of choice because it has an intermediate binding energy to many carbon-based species[22]. This is a favorable metric in CO_2 reduction because it enables the retention of surface intermediates en route to the formation of highly reduced products like ethylene while not binding them too strongly to poison the surface. Thus, we reasoned that the same argument would apply in retaining CO_2 reduction intermediates long enough for their coupling with NH_3 would hold. While there is a plethora of studies of Cu-based catalysts and how defects, surface crystallographic facets, ligands, oxygen species and more dictate reaction pathways, we chose to leave such catalyst modifications for future follow-up works given the novelty of this reaction path[22]. The one variable that we did choose to investigate was the use of CuO as a starting material, which when reduced to Cu under cathodic potentials would likely contain additional binding sites in the form of defects. As such, Cu (Fig. 2a) and CuO (Fig. 2b) with no deliberate surface or structural modifications and size around 100 nm were used. The catalysts were mixed with a nafion binder to generate an ink which was then drop cast onto a gas diffusion electrode. This type of electrode featured a gas-permeable gas diffusion layer and microporous layer through which CO_2 could reach the catalyst layer on top (Fig. 2c) with the goal being to drive the C-N coupling reaction at the interfacial triple-phase boundary. The particular type of electrode geometry is particularly beneficial in overcoming the limited solubility of CO_2 in aqueous electrolyte, enabling the use of alkaline electrolytes that minimize the competing hydrogen evolution reaction, and thus attaining industrially relevant current densities (hundreds of mA/cm^{-2}) [23,24].

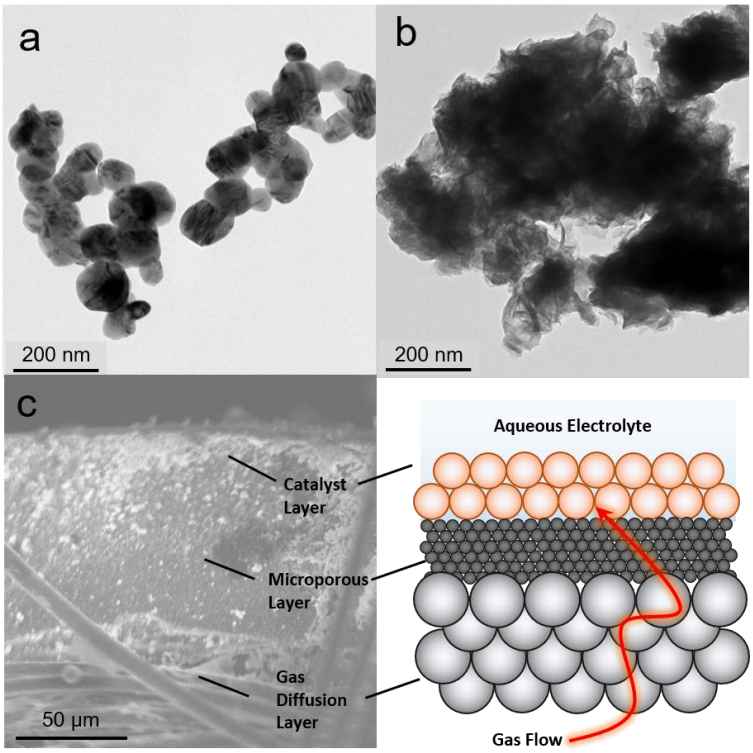

Figure 2: Transmission electron microscopy images of Cu (a) and CuO (b) catalysts and their assembly on a gas diffusion electrode (c).

Electrosynthetic Studies:

We employed 1M KOH as an electrolyte for this work as highly alkaline electrolytes tend to minimize the hydrogen evolution reaction (HER) and thus favor CO_2 reduction. NH_3 was set to be a model nitrogen source. In the long term, NH_3 would ideally be replaced directly by N_2 as an abundant feedstock, though at this stage, electrochemically activating N_2 not yet a well-established reaction[25,26]. Formamide (Fig. 3a) and acetamide (Fig. 3b) primary amines were two likely C-N coupled products that could be formed from NH_3 and C_1 and C_2 surface intermediates via several proton and electron transfer steps. In a gas-diffusion based electrochemical cell, both Cu and CuO featured an onset of catalytic current around 0V vs. the reversible hydrogen electrode (RHE) and reached 100 mA/cm^2 by $-1.0V_{RHE}$ (Fig. S1 a,b). The addition of NH_4OH (present as mainly NH_3 in alkaline solutions) to the electrolyte did not significantly alter the current density. Product quantification with gas chromatography (GC) and NMR revealed formate and H_2 to be the two main products from the reaction (Fig. S2). However, on both Cu and CuO, formamide and acetamide were detected and were formed with partial current densities of ranging from 0.1 to 1.2 mA/cm^2, depending on the applied potential (Fig. 3c, d). While the Faradaic efficiency for their formation was rather modest, peaking at approximately 1% (Fig. 3e, f), this study constitutes the first report of their synthesis from CO_2 and NH_3 building blocks. In addition, performing the same measurements in a standard 3-electrode setup with the working electrode completely immersed in the aqueous phase did not result in any detectible C-N products, even after 24 hrs of electrolysis. As a control experiment, CO_2 electrolysis alone only resulted in formate (Fig. 3g) and acetate (Fig. 3h) products that gave rise to NMR peaks in the range of interest. Interestingly, while the formate selectivity was very high (up to 90%) without NH_3, NH_3 addition to the electrolyte decreased this value by a factor of 2-3 (Fig. S3). While this performance is not yet sufficient for economically competitive electrosynthesis, improving the initial system should certainly be feasible as one could point to the rapid maturation of CO_2 electrosynthetic technologies over the last decade[2].

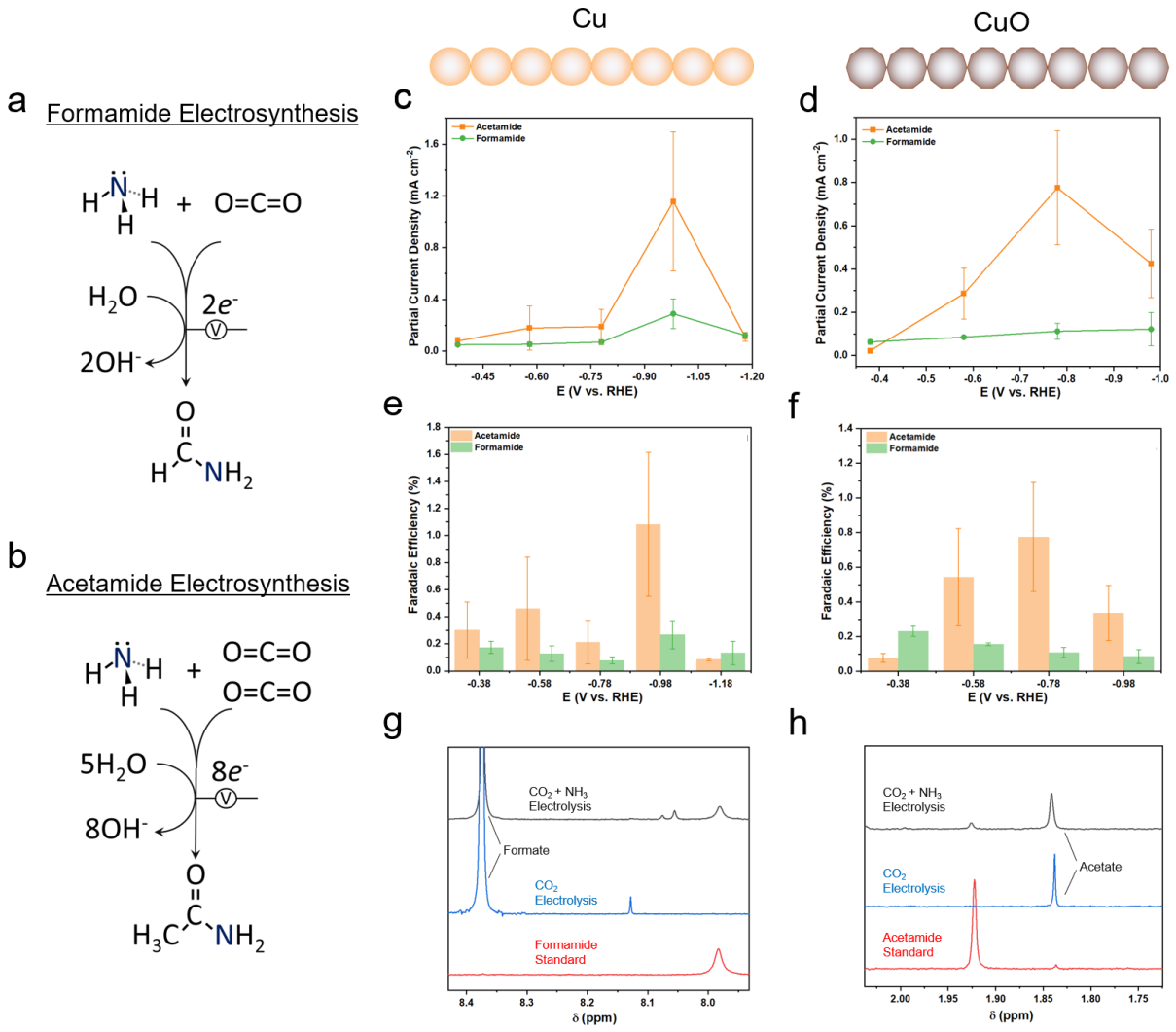

Figure 3: Electrosynthetic reaction pathways to formamide (a) and acetamide (b). Partial current density of C-N products formed over Cu (c) and CuO (d) catalysts. Faradaic efficiencies maximized around 1% for acetamide and 0.2% for formamide on Cu (e) and CuO (f). Control experiments with CO_2 electrolysis did not show any formamide (g) or acetamide (h) formation.

Infrared Spectroscopy

To extract a further level of insights into the formamide and acetamide electrosynthetic pathways, we turned to infrared spectroscopy. The spectroscopic measurements were carried out in an attenuated-total reflection (ATR) mode using a home-built spectroelectrochemical setup (Fig. 4a). Briefly, a thin layer of aqueous electrolyte (KOH or KOH + NH_3) was on top of the diamond-coated ZnSe ATR crystal. The Cu catalyst layer/microporous layer/gas diffusion layer composite electrode was placed overtop so that the gas/liquid/solid triple-phase boundary could be spectroscopically probed. The ability to probe this region was evident when measuring the difference spectrum between Ar flow and CO_2 flow in this

configuration, which shows the presence of both gaseous and dissolved CO_2 and carbonate species (Fig. S10, 11)[27].

Next, spectra under catalytic conditions, across a representative range of applied current densities, were recorded using the spectrum under open circuit conditions as the background. Under an argon flow with NH_3 present using a CuO catalyst, the main spectral features corresponded mainly to that of water (bands at 1620 and 3400 cm^{-1}) and to that of NH_3 (bands at 1100 and 3300 cm^{-1}), indicating that adsorption and desorption of these molecules was taking place (Fig. 4b) [27]. Under the same conditions but with CO_2 flowing in place of Ar, a new set of positive bands appeared (1660, 1300, 1004, and 840 cm^{-1}) alongside of a negative band 1403 cm^{-1}) (Fig. 4c). Generally, the addition of spectral features corresponds to both catalytic effects (formation of surface intermediates, products) and electrolyte effects (changes in carbonate/bicarbonate concentrations) [28]. While carbonate/bicarbonate was not explicitly added, it has been shown to spontaneously appear at the gas-liquid interface in similar conditions, alongside of a near-neutral interfacial pH.[29] The rise of a strong band at 1300 and decrease of 1400 may stem from changes in HCO_3^-/CO_3^{2-} species as these species have dominant bands here (S10, 11)[27]. However, bands around 1660 and 1300-1400 cm^{-1} have also been attributed to C=O and C-O stretches of surface-bound species and this may also contribute to spectral intensity here, given that formate is the primary CO_2R product observed[30-32]. While the precise mechanism of formate electrosynthesis is still under debate, on copper surfaces, it has been argued through a combination of surface-enhanced Raman spectroscopy (observed intermediate bands at 1500-1600 cm^{-1}) and DFT modelling that the all CO_2 reduction pathways share a common first intermediate in a μ_2, -C, -O bound CO_2^{*-} that subsequently gets hydrogenated en route to formate or protonated to *COOH en route to CO and other C_2 downstream products[33]. As such, our electrosynthetic route may proceed through this proposed pathway.While spectral features in the 1800-2100 cm^{-1} are noted where the C-O stretch of *CO is located, the inherent absorbance of our diamond-coated ATR crystal makes this region rather noisy rendering bands here more difficult to fit and explicitly assign.

In the presence of both CO_2 and NH_3, new bands appeared at both the region containing N-H bonds (2800-3200 cm^{-1}) and C-N bonds (1459 cm^{-1}) (Fig. 4d). In fact, bands at similar positions were previously noted under electrochemical co-reduction of CO_2 and N_2 en route to urea synthesis on $Pd/Cu/TiO_2$ catalysts[15]. The intensity of these bands rose as current increased, indicating the continual buildup of these intermediates and their formation (rather than their desorption) as a likely limiting step. As a method of validation, spectra were also acquired with $^{15}NH_3$ instead of $^{14}NH_3$ (Fig. 4e). Indeed, the isotope effect was noted via a red-shift around 30 cm^{-1} of the N-H and C-N bands. To glean a further layer of mechanistic detail, we plotted the normalized area of the observed bands in the measured spectra vs. the current of the electrode. Interestingly, the intensity of the band at 1300 cm^{-1}, likely corresponding to bicarbonate, saturated very early with only CO_2 present, but continually gained intensity under increasingly higher currents when NH_3 was present (Fig. 4f). A possible explanation for this could that be the presence of NH_3 diminishes the concentration of CO_2/carbonate reactants near the interface at low current densities and thus pushes the selectivity from formate to hydrogen. Finally, as (bi)carbonate species dominate the IR spectra, we opted to subtract spectra of the catalyst systems operating at -20 mA from those at -200 mA, as the (bi)carbonate species are mostly saturated and those with smaller spectral contributions could be visualized (Fig. 4g). Indeed, we noted a main positive band at 1392 cm^{-1} for CuO/CO_2 while $CuO/CO_2/NH_3$ featured positive bands at 1548 and 1404 cm^{-1} and negative bands at 1423 and 1361 cm^{-1}. Further, Cu/CO_2 displayed positive bands at 1423, 1399 and 1101 cm^{-1} and negative bands at 1361 and 1015 cm^{-1} while $Cu/CO_2/NH_3$ had a main lone band 1393 and several negative bands at 1262, 1091, 1018 and 798 cm^{-1}. While a fully unambiguous assignment at this stage is not yet possible, we note that each of these spectra feature a main band around 1393-1400 cm^{-1} which has previously been assigned to the C-O symmetric stretch of $*COO^-$ [30-32]. As formate is the dominant product in each of these systems,

it would seem reasonable to have a substantial *COO^- surface coverage and thus this is our tentative assignment.

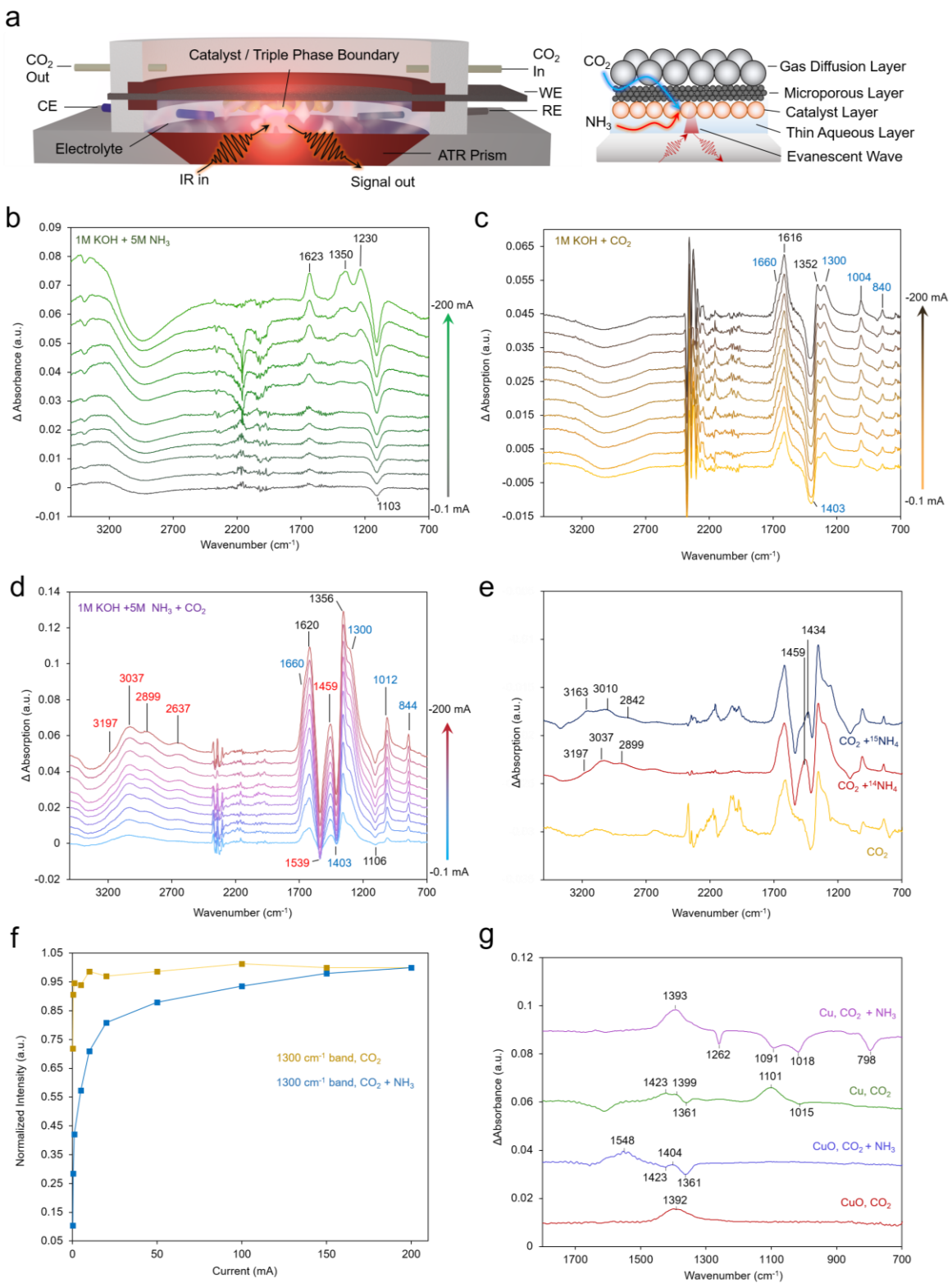

Figure 4: Spectroelectrochemical setup enabling *operando* infrared spectroscopic probing of the electrosynthetic reactions in a gas-diffusion electrode cell (a). Difference spectra (with the system at open circuit as the background), of CuO with KOH + NH_3 (b), KOH + CO_2 (c), and KOH + NH_3 + CO_2 (d). Spectra at 50 mA were also acquired with $^{15}NH_3$ to validate assignments of N-H and C-N stretches (e). The rise of the 1300 cm^{-1} band follows a different current-intensity profile in the absence vs. presence of NH_3 (f). Subtracting the spectra at -20 mA from those at -200 mA enables the identification of additional species present within the system (g).

We believe that the formate and formamide electrosynthetic pathways are linked on the Cu surface in that they share a common intermediate. This belief is backed by their similarity in chemical structure and by the observation that the presence of ammonia specifically decreases the formate selectivity (Fig. S3), which would occur if the part of the reaction ended up diverting from formate to formamide. Considering that the formation of C-N containing products involves the nucleophilic attack of a carbon atom by the lone pair on the nitrogen atom of ammonia, an activated, yet exposed carbon species that could couple with ammonia for formamide generation could be that of the μ_2, -C, -O bound CO_2*[-33]. There would then be a competition between hydrogenation of this species to produce formate or a nucleophilic attack to eventually form formamide (Fig. 5a). On the other hand, acetamide synthesis likely shares a reaction pathway with acetate and thus requires a C_2 intermediate to already be present[16]. The *CCO intermediate was recently proposed as a likely candidate for this through a DFT analysis of acetamide synthesis via CO and NH_3 building blocks and would be a plausible candidate for our work as well (Fig. 5b) [16]. The middle carbon would thus be subject to nucleophilic attack by the NH_3 in this pathway where it diverges from the acetate pathway. The two pathways presented here are not so different than what occurs in enzymatic catalytic pockets, where an electron rich amine couples with an electron poor carbon[10-12] and one can imagine that generating on-surface catalytic pockets in a synthetic system to promote this reaction would lead to further enhancements of electrosynthetic selectivity.

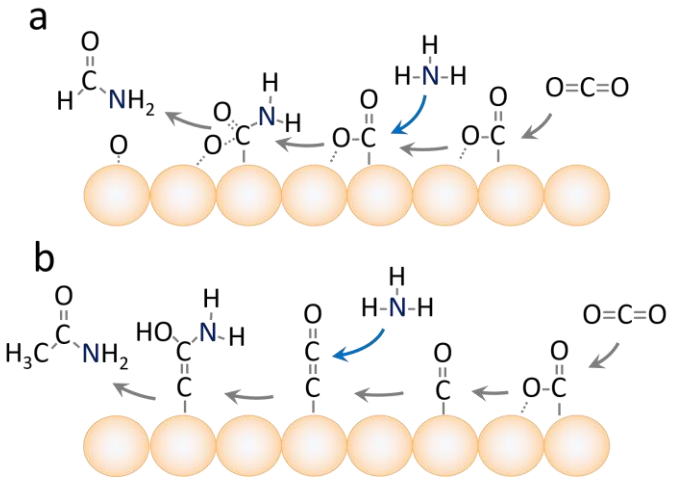

Figure 5: Plausible surface reaction pathways in the electrosynthetic process of formamide (a) and acetamide (b) generation.

Concluding Remarks:

While two new reaction pathways have been discovered in formamide and acetamide electrosynthesis using CO_2 and NH_3 building blocks, many avenues are now opened for further understanding and improving the efficiency of these reactions. First, while we used commercially purchased Cu and CuO nanoparticles as a readily available model system, they feature a diversity of active sites, defects, (sub)surface oxygen species, and exposed crystallographic facets and it is entirely possible that each of these factors may influence the reaction like they do in the electrosynthesis of carbon-based products via CO_2 reduction. A rational way forward would be the precise study of well-defined copper catalysts in which the nature surface-active sites are known and with complementary theoretical modelling of likely reaction pathways on these surfaces. Further, it is not known if Cu is the only catalyst capable of carrying out this reaction and if formate-selective metals like Sn and Bi would thus be more effective at formamide synthesis. In addition, we have developed an *operando* infrared spectroscopic method for the first time that was used to help understand this reaction pathway but additional complementary techniques such as Raman and X-ray absorption would contribute immensely valuable pieces to this puzzle[34].

This principal significance to this work is the electrosynthetic reaction discovery which we envision will accelerate the adoption of electrosynthetic methodology at large in both the academic and industrial domains. While NH_3 is used as the model nitrogen source, eventually, this may be replaced by N_2 in a fully sustainable nitrogen cycle. In general, the capacity to drive heteroatomic surface coupling reactions with renewable-electricity powered systems stands to open up an abundance of decentralized green synthetic routes in place of heavy-infrastructure requiring fossil fuel based thermochemical approaches. In parallel, there is much more fundamental chemistry to be discovered through the use of new interfaces, spectroscopic methodology, and catalytic systems.

Acknowledgements:

N.K. and J.L acknowledge NSERC Discovery Grant RGPIN-2019-05927

Author Contributions:

N.K and J.L both designed the project, carried out experiments, processed data, contributed intellectual insights and wrote the manuscript.

Competing Interests:

None to declare

References:

1 Masa, J., Andronescu, C. & Schuhmann, W. Electrocatalysis as the Nexus for Sustainable Renewable Energy: The Gordian Knot of Activity, Stability, and Selectivity. *Angew. Chem. Int. Ed.* **59**, 15298-15312 (2020).

2 De Luna, P. *et al.* What would it take for renewably powered electrosynthesis to displace petrochemical processes? *Science* **364**, eaav3506 (2019).

3 Wang, M. *et al.* Can sustainable ammonia synthesis pathways compete with fossil-fuel based Haber–Bosch processes? *Energy Environ. Sci.* (2021).

4 Kibsgaard, J. & Chorkendorff, I. Considerations for the scaling-up of water splitting catalysts. *Nat. Energy* **4**, 430-433 (2019).

5 Ross, M. B. *et al.* Designing materials for electrochemical carbon dioxide recycling. *Nat. Catal.* **2**, 648-658 (2019).
6 Afanasyev, O. I., Kuchuk, E., Usanov, D. L. & Chusov, D. Reductive Amination in the Synthesis of Pharmaceuticals. *Chemical Reviews* **119**, 11857-11911 (2019).
7 Dunetz, J. R., Magano, J. & Weisenburger, G. A. Large-Scale Applications of Amide Coupling Reagents for the Synthesis of Pharmaceuticals. *Organic Process Research & Development* **20**, 140-177 (2016).
8 Guo, X., Facchetti, A. & Marks, T. J. Imide- and Amide-Functionalized Polymer Semiconductors. *Chemical Reviews* **114**, 8943-9021 (2014).
9 Höhne, M. & Bornscheuer, U. T. Biocatalytic Routes to Optically Active Amines. *ChemCatChem* **1**, 42-51 (2009).
10 Patil, M. D., Grogan, G., Bommarius, A. & Yun, H. Oxidoreductase-Catalyzed Synthesis of Chiral Amines. *ACS Catal.* **8**, 10985-11015 (2018).
11 Mayol, O. *et al.* A family of native amine dehydrogenases for the asymmetric reductive amination of ketones. *Nat. Catal.* **2**, 324-333 (2019).
12 Aleku, G. A. *et al.* A reductive aminase from Aspergillus oryzae. *Nat. Chem.* **9**, 961-969 (2017).
13 Kim, H. & Chang, S. Transition-Metal-Mediated Direct C–H Amination of Hydrocarbons with Amine Reactants: The Most Desirable but Challenging C–N Bond-Formation Approach. *ACS Catal.* **6**, 2341-2351 (2016).
14 Kim, J. E., Choi, S., Balamurugan, M., Jang, J. H. & Nam, K. T. Electrochemical C-N Bond Formation for Sustainable Amine Synthesis. *Trends Chem.* **2**, 1004-1019 (2020).
15 Chen, C. *et al.* Coupling N2 and CO2 in H2O to synthesize urea under ambient conditions. *Nat. Chem.* **12**, 717-724 (2020).
16 Jouny, M. *et al.* Formation of carbon–nitrogen bonds in carbon monoxide electrolysis. *Nat. Chem.* **11**, 846-851 (2019).
17 Meng, N., Huang, Y., Liu, Y., Yu, Y. & Zhang, B. Electrosynthesis of urea from nitrite and CO2 over oxygen vacancy-rich ZnO porous nanosheets. *Cell Rep. Phys. Sci.* **2**, 100378 (2021).
18 Feng, Y. *et al.* Te-Doped Pd Nanocrystal for Electrochemical Urea Production by Efficiently Coupling Carbon Dioxide Reduction with Nitrite Reduction. *Nano Lett.* **20**, 8282-8289 (2020).
19 Roylance, J. J. & Choi, K.-S. Electrochemical reductive amination of furfural-based biomass intermediates. *Green Chemistry* **18**, 5412-5417 (2016).
20 Shibata, M., Yoshida, K. & Furuya, N. Electrochemical Synthesis of Urea at Gas-Diffusion Electrodes: IV. Simultaneous Reduction of Carbon Dioxide and Nitrate Ions with Various Metal Catalysts. *Journal of The Electrochemical Society* **145**, 2348-2353 (1998).
21 Fukushima, T. & Yamauchi, M. Electrosynthesis of amino acids from biomass-derivable acids on titanium dioxide. *Chemical Communications* **55**, 14721-14724 (2019).
22 Nitopi, S. *et al.* Progress and Perspectives of Electrochemical CO2 Reduction on Copper in Aqueous Electrolyte. *Chemical Reviews* **119**, 7610-7672 (2019).
23 Higgins, D., Hahn, C., Xiang, C., Jaramillo, T. F. & Weber, A. Z. Gas-Diffusion Electrodes for Carbon Dioxide Reduction: A New Paradigm. *ACS Energy Lett.* **4**, 317-324 (2019).
24 García de Arquer, F. P. *et al.* CO2 electrolysis to multicarbon products at activities greater than 1 A cm2. *Science* **367**, 661-666 (2020).
25 Foster, S. L. *et al.* Catalysts for nitrogen reduction to ammonia. *Nat. Catal.* **1**, 490-500 (2018).
26 Liu, D. *et al.* Development of Electrocatalysts for Efficient Nitrogen Reduction Reaction under Ambient Condition. *Advanced Functional Materials* **31**, 2008983 (2021).
27 Milella, F. & Mazzotti, M. Estimating speciation of aqueous ammonia solutions of ammonium bicarbonate: application of least squares methods to infrared spectra. *React. Chem. Eng.* **4**, 1284-1302 (2019).

28 Kas, R. *et al.* In-Situ Infrared Spectroscopy Applied to the Study of the Electrocatalytic Reduction of CO2: Theory, Practice and Challenges. *ChemPhysChem* **20**, 2904-2925 (2019).
29 Lu, X. *et al.* In Situ Observation of the pH Gradient near the Gas Diffusion Electrode of CO2 Reduction in Alkaline Electrolyte. *J. Am. Chem. Sci.* **142**, 15438-15444 (2020).
30 Baruch, M. F., Pander, J. E., White, J. L. & Bocarsly, A. B. Mechanistic Insights into the Reduction of CO2 on Tin Electrodes using in Situ ATR-IR Spectroscopy. *ACS Catal.* **5**, 3148-3156 (2015).
31 Firet, N. J. & Smith, W. A. Probing the Reaction Mechanism of CO2 Electroreduction over Ag Films via Operando Infrared Spectroscopy. *ACS Catal.* **7**, 606-612 (2017).
32 Zhu, S., Jiang, B., Cai, W.-B. & Shao, M. Direct Observation on Reaction Intermediates and the Role of Bicarbonate Anions in CO2 Electrochemical Reduction Reaction on Cu Surfaces. *J. Am. Chem. Sci.* **139**, 15664-15667 (2017).
33 Chernyshova, I. V., Somasundaran, P. & Ponnurangam, S. On the origin of the elusive first intermediate of CO2 electroreduction. *Proc. Natl. Acad. Sci. U.S.A.* **115**, E9261 (2018).
34 Zhu, Y., Wang, J., Chu, H., Chu, Y.-C. & Chen, H. M. In Situ/Operando Studies for Designing Next-Generation Electrocatalysts. *ACS Energy Lett.* **5**, 1281-1291 (2020).

Supplementary information for:

Electrochemically Driven C-N Bond Formation from CO_2 and Ammonia at the Triple-Phase Boundary

Junnan Li[a] and Nikolay Kornienko[a]*

[a]*Department of Chemistry, Université de Montréal, 1375 Ave. Thérèse-Lavoie-Roux, Montréal, QC H2V 0B3*

*email: Nikolay.kornienko@umontreal.ca

Characterization:

Scanning electron microscopic (SEM) images and EDS were measured using a JEOL JSM-7600F Field Emission SEM microscope. Transmission electron microscopic (TEM) images were performed on JEOL JEM-2100F FEG-TEM, operated at 200 kV.

Electrochemistry and product quantification:

Linearly sweep voltammetry (LSV) was accomplished using a Bio-Logic SP-200 Potentiostat (BioLogic Science Instruments, France). A three-electrode system has been employed by applying the carbon cloth gas diffusion layer (GDL-CT (W1S1009, Fuel Cells Etc.) as the working electrode, Ag/AgCl as the reference electrode and a glassy carbon rod as the counter electrode.

The preparation of working electrode followed steps below: 10 mg Cu (Alfa Aesar, Copper Nanopowder, 99.9% APS 20-50 nm, Lot P11F044) or CuO (Alfa Aesar, Copper(II) Oxide, nanopowder, Lot Y19E022) commercial powder was added into a mixture with 100 μL H_2O, 300 μL ethanol, 25 μL Nafion. After ultrasonic mixing for 10 minutes, 100 μL catalyst ink was dropped onto the carbon cloth and allowed to dry naturally under ambient conditions. 1M KOH solution with different amounts of NH_4OH was used as the electrolyte in all of the measurements. The LSVs were measured in the range of 0.7 ~ -0.98 V (vs. RHE) at a sweep rate of 20 mV s^{-1}. Potentiostatic electrolysis was conducted in a gas diffusion electrode (GDE) cell. Before each electrolysis experiment, 1 mL electrolyte was added into the cell, the flow rate of CO_2 is 6mL/min. All reactions were carried out at room temperature (23 ± 1 °C). Bulk electrolysis was carried out with 1M NH_3 for Cu and 5M NH_3 for CuO as these were the experimentally optimized conditions for C-N product generation rates. In order to analyze the products of the reaction, gas chromatography (GC, SRI 8610C) and NMR (Bruker AVANCE II 400 se) were performed to reveal the content and composition of the gas and liquid products respectively. A sealed GDE cell

was used and connected with the GC. The CO_2 flow rate employed was 6 mL/min. 400 μL liquid product was mixed with 400 μL D_2O to test the NMR and quantify liquid products. Typically, liquid products were acquired after 30 minutes of electrolysis.The faradaic efficiency (FE) was calculated by using the following formula:

$$\varepsilon_{FE} = \frac{\alpha n F}{Q}$$

where α is electron transfer numbers, n is the moles of the products, F is the Faraday constant (96485 C mol^{-1}), Q is the charge passed in total during the reaction.

In-situ infrared (IR) spectroscopy:

IR spectra were acquired on a ThermoFischer Nicolet 380 FTIR-ATR with a ZnSe ATR crystal that was coated with a diamond surface. Typically, 200 scans were acquired for each measurement. A three-electrode GDE cell was used for the in-situ IR experiment. Cu wire was used as counter electrode, Ag/AgCl was used as reference, the above carbon cloth with CuO or Cu as working electrode. The electrolyte employed was 1M KOH with or without NH_4OH under a constant CO_2 gas flow. The catalyst, deposited onto a carbon cloth gas diffusion layer (coated with a microporous layer) was facing downwards towards the ATR crystal, with a thin electrolyte layer between. The working electrode was gently pressed with a porous foam stud so that there was still ample gas permeation into the triple-phase boundary that was being probed with the IR evanescent wave.

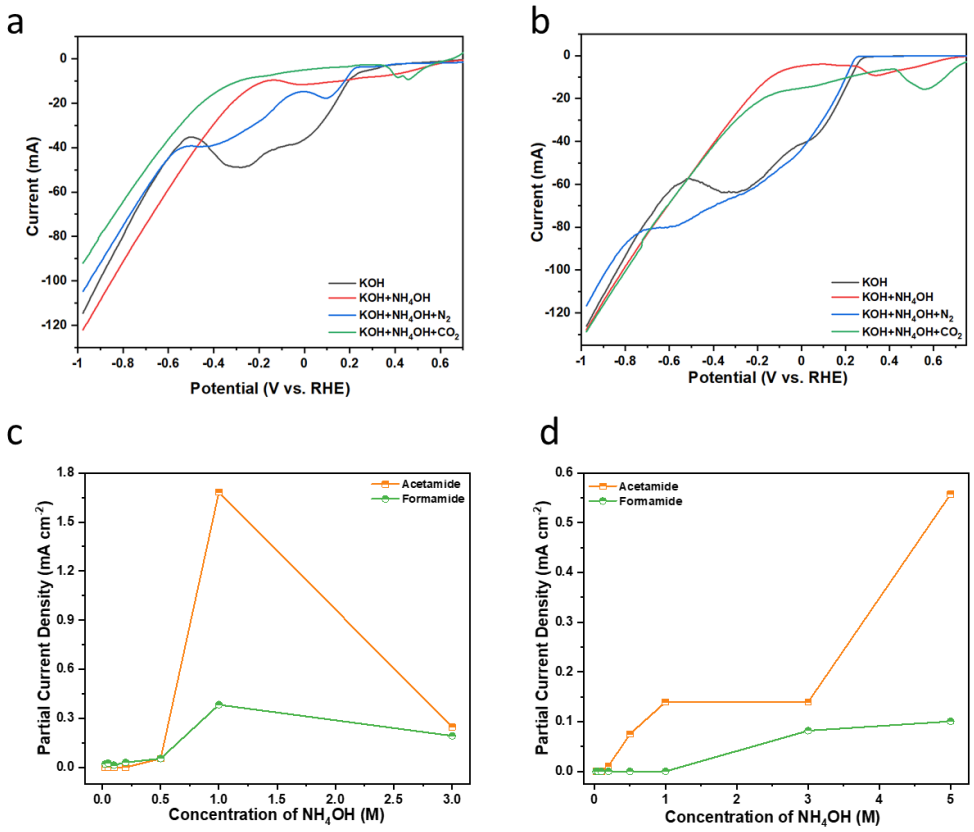

Figure S1. LSV curves under different gas environment of (a) Cu; (b) CuO catalyst in different electrolytes. Partial current densities for C-N products from an initial screening of selecting optimal NH_4OH concentrations to add to the electrolyte were also different for Cu (c) and CuO (d).

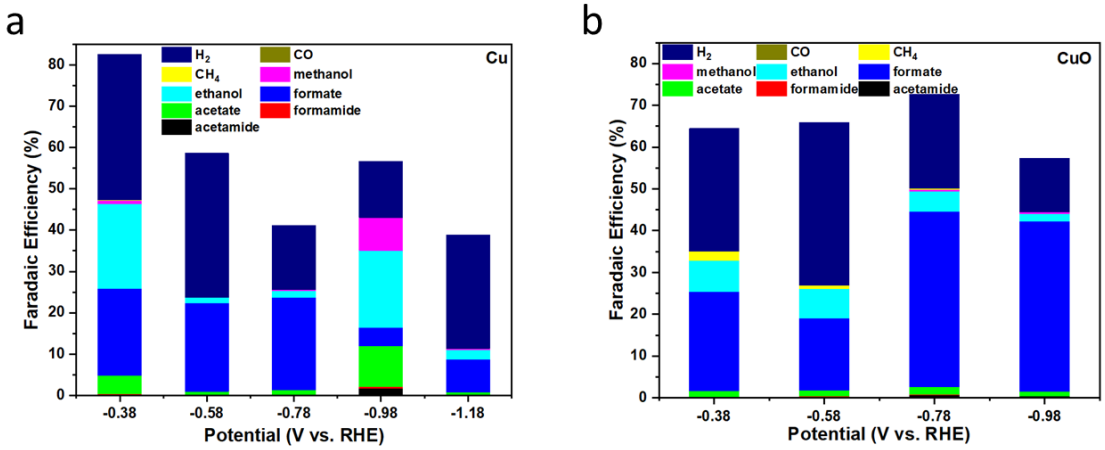

Figure S2: Total product quantification for Cu (a) and CuO (b) catalysts.

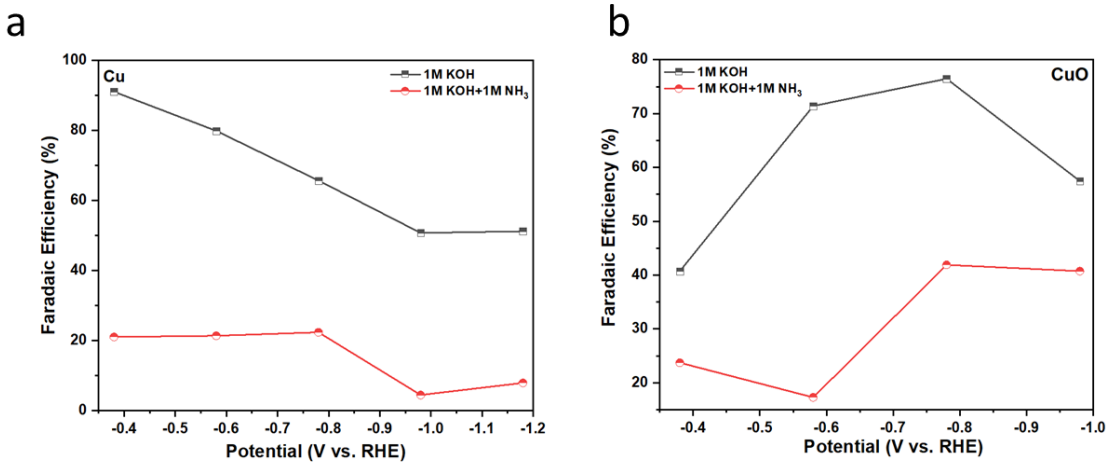

Figure S3: Faradaic efficiency for formate production in the absence and presence of NH_3 for Cu (a) and CuO (b) catalysts

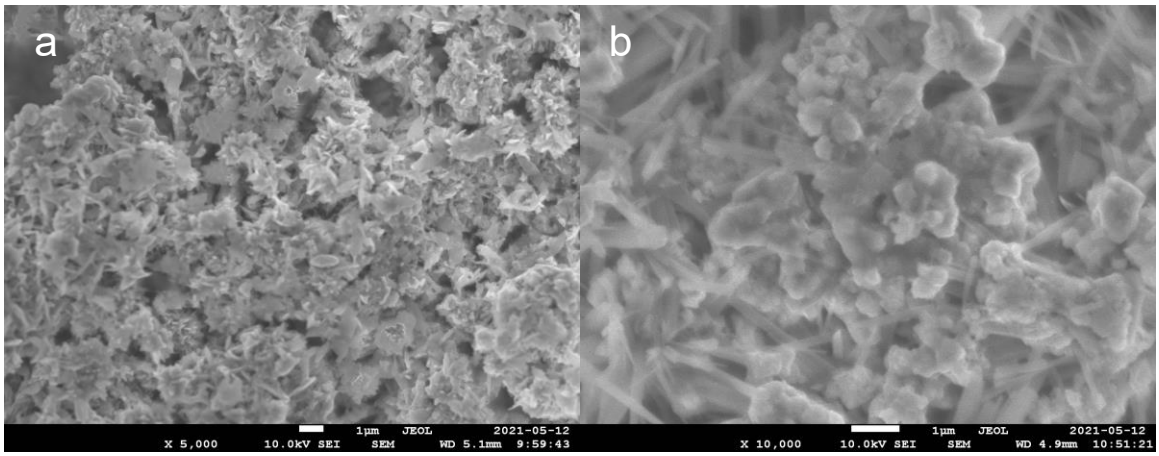

Figure S4. SEM images of (a) CuO and (b) Cu after a typical controlled potential electrolysis reaction.

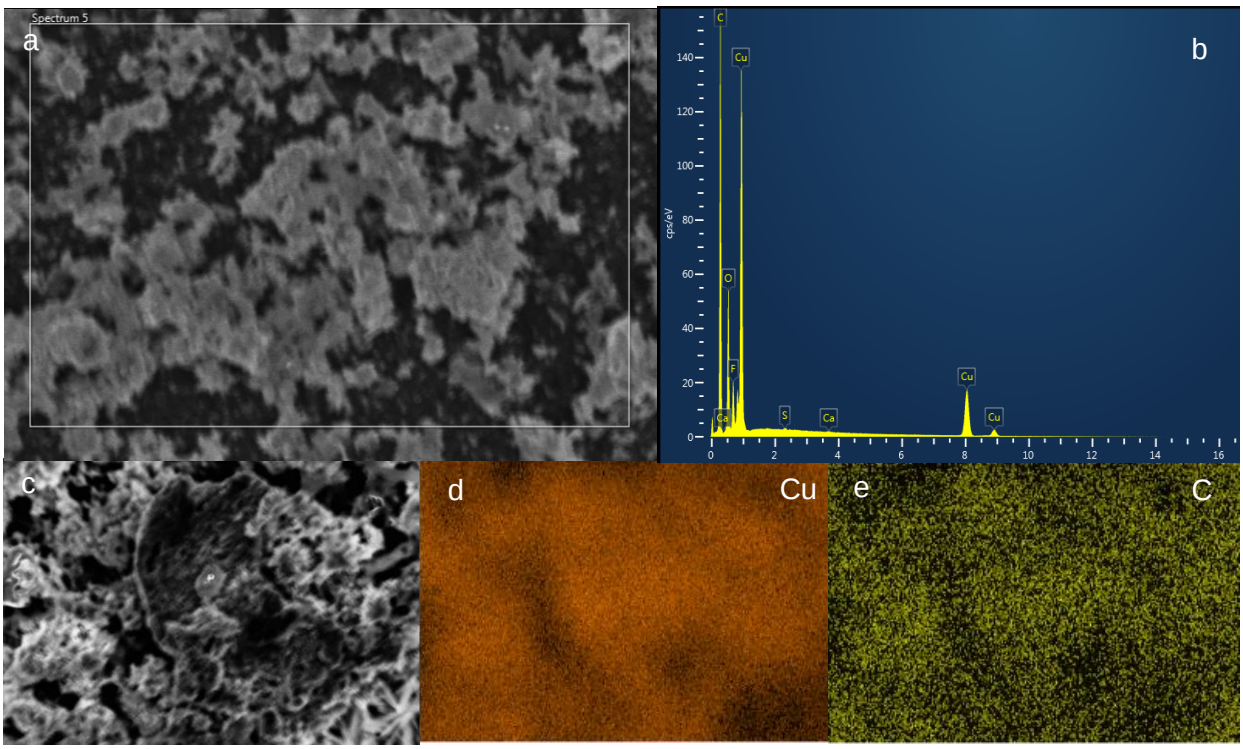

Figure S5. (a, c) SEM images of the EDS area; EDS of CuO/C catalyst before reaction (b) EDS spectra; (d) Cu and (e) C element mapping after reaction**.**

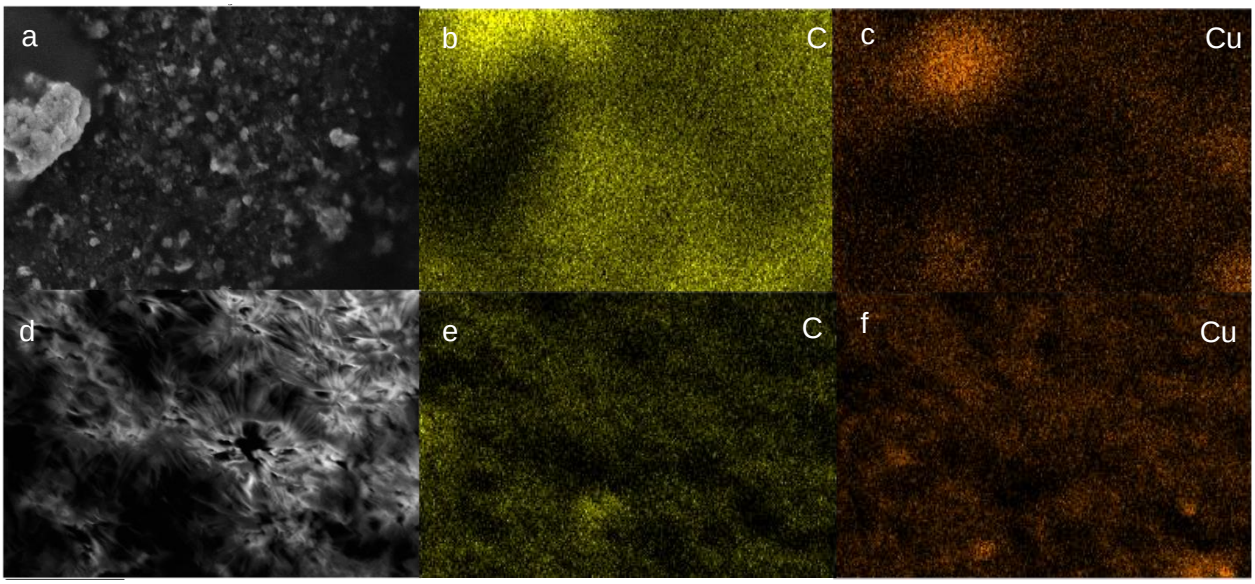

Figure S6. (a, c) SEM images of the EDS area; (b) C and (c) Cu element EDS mapping of Cu/C catalyst before reaction ; (d) C and (f) Cu after reaction.

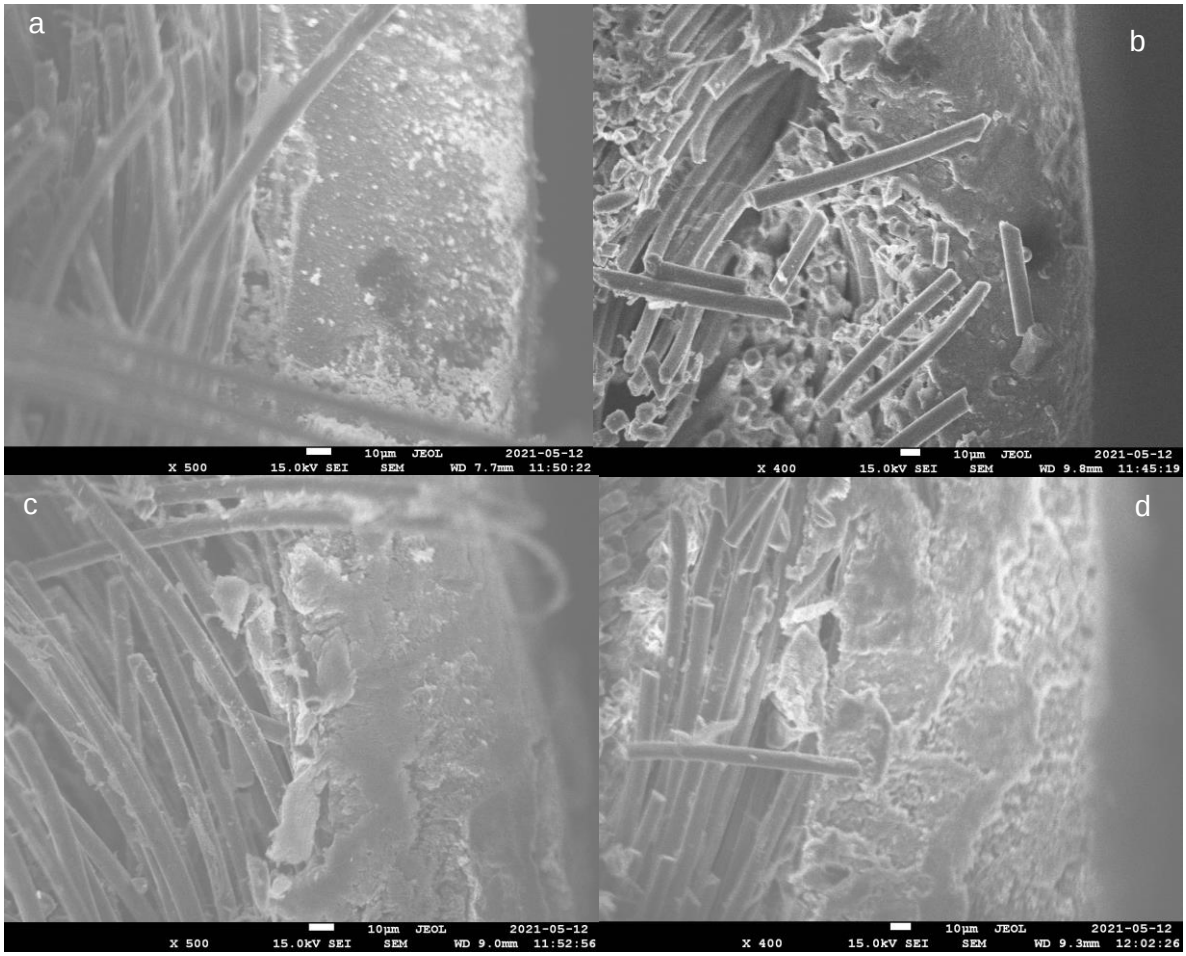

Figure S7. SEM images of the cross session (a) CuO/C before reaction; (b) CuO/C after reaction; (c) Cu/C before reaction; (d) Cu/C after reaction.

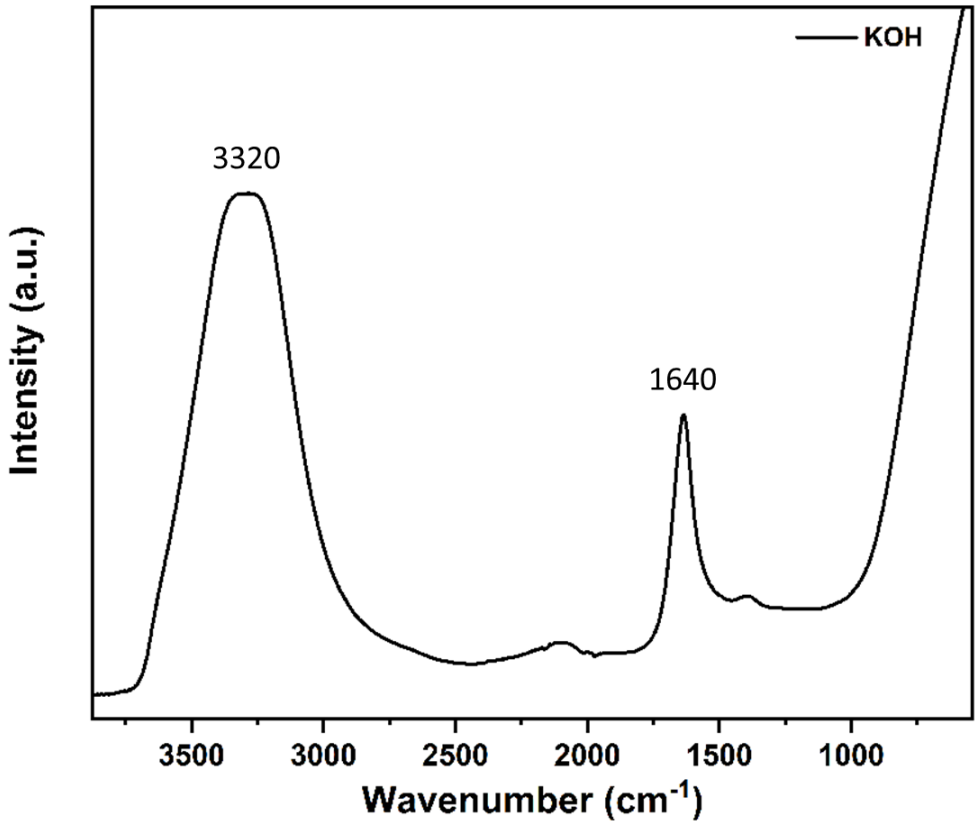

Figure S8: IR spectrum of 1M KOH

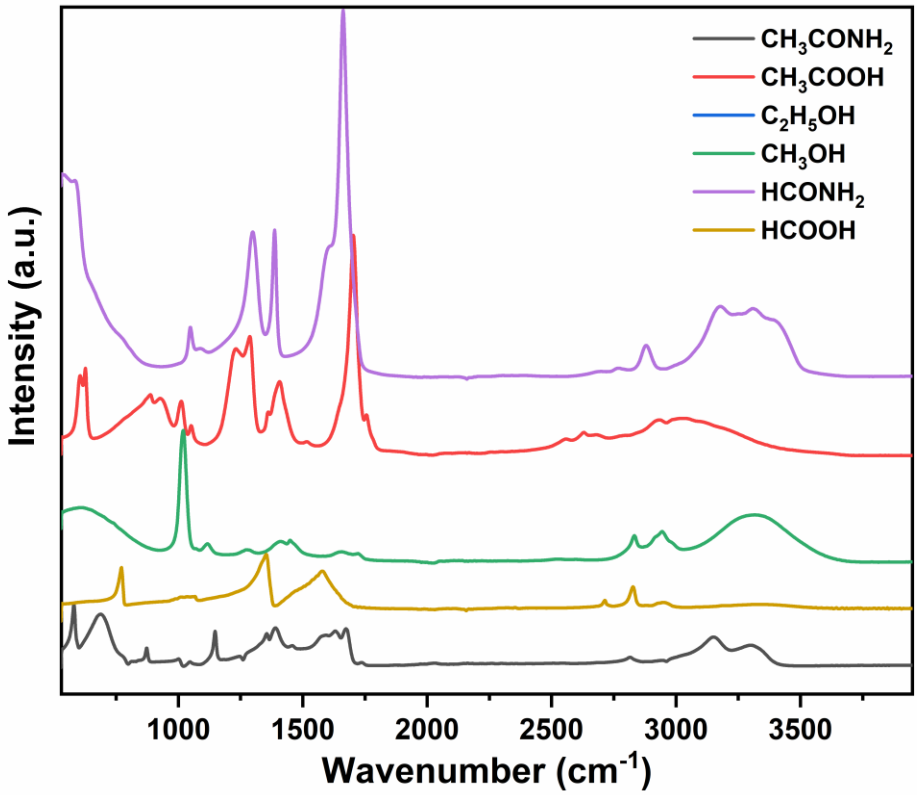

Figure S9: IR spectra of several products detected in NH_3 + CO_2 electrolysis

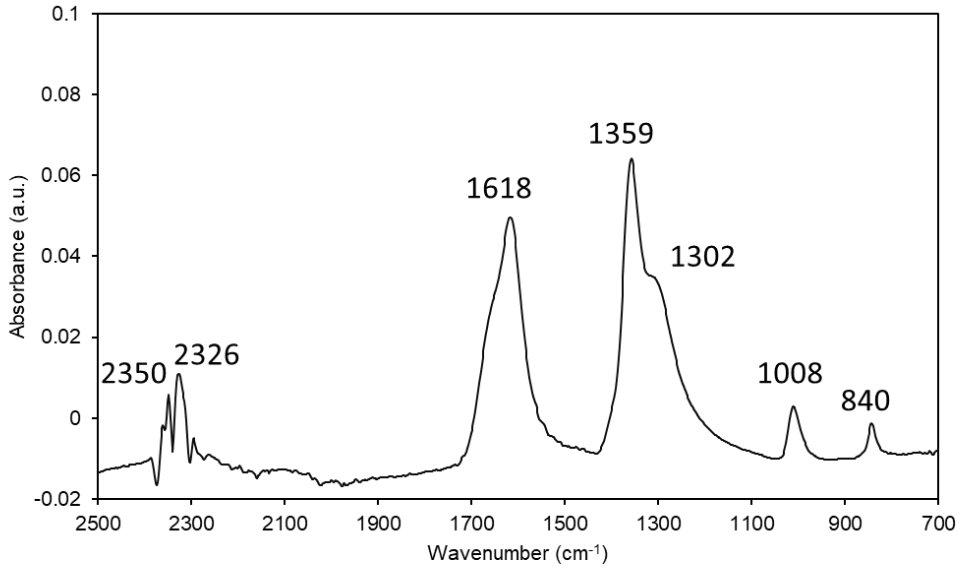

Figure S10: IR spectrum of the spectroelectrochemical setup with a CO_2 flow in 1M KOH, using an Ar flow in 1M KOH as the background. Peaks attributable to CO_2 and carbonate are present.

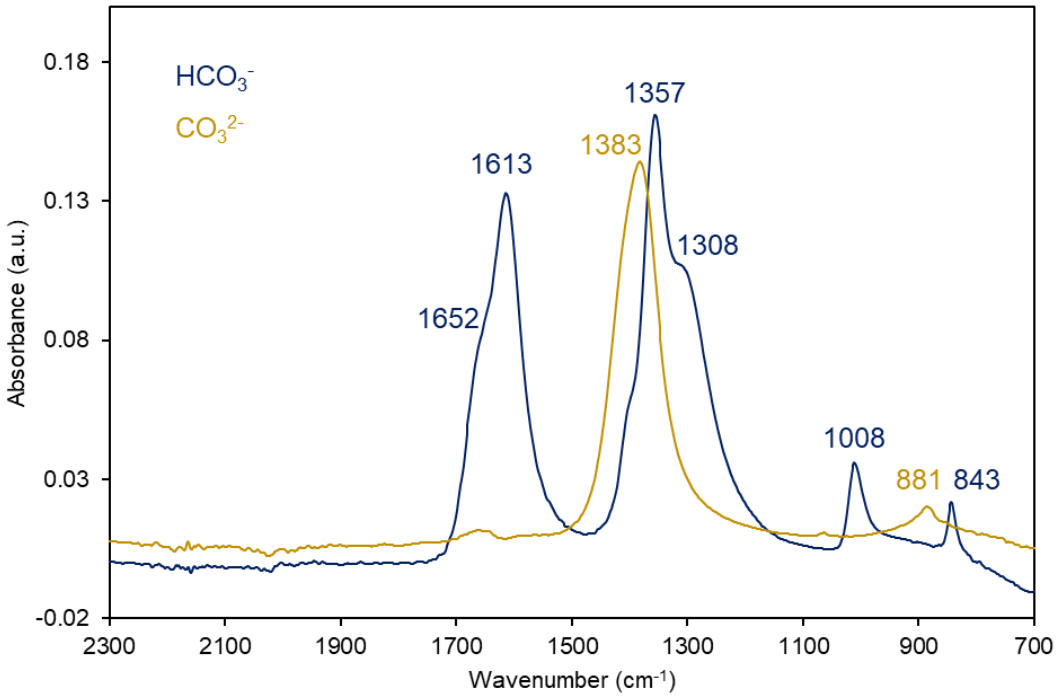

Figure S11: IR spectra of $KHCO_3$ and K_2CO_3 dissolved in water

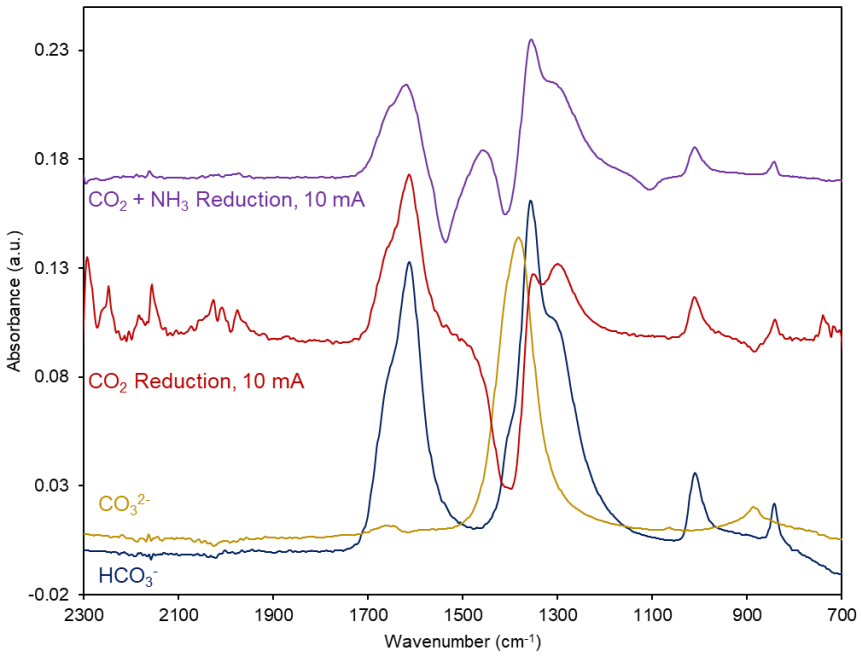

Figure S12: Overlaid spectra of (bi)carbonate and CO_2 reduction

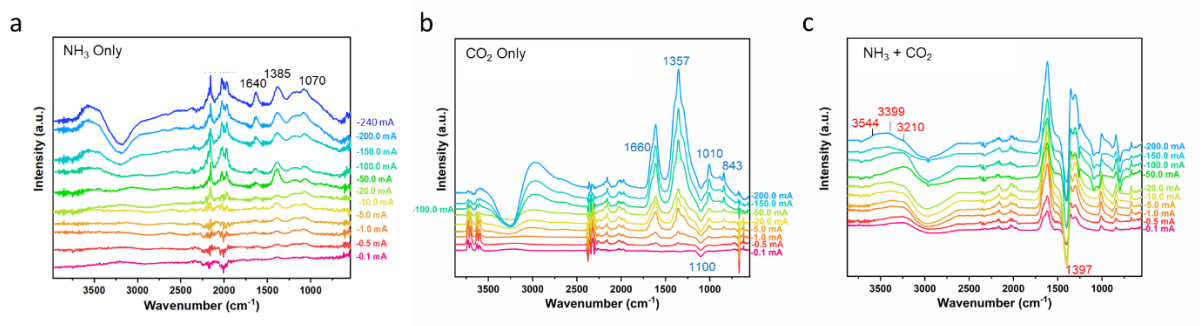

Figure S13: IR spectra of Cu catalysts, with NH_3 only (a), CO_2 only (b), and NH_3 + CO_2 (c).